Calibration of Optical Tweezers for In Vivo Force Measurements: How do Different Approaches Compare?

5 AUTHORS, INCLUDING:

Yonggun Jun
University of California, San Diego
29 PUBLICATIONS 167 CITATIONS

SEE PROFILE

Babu Reddy J Narayanareddy
University of California, Irvine
21 PUBLICATIONS 96 CITATIONS

SEE PROFILE

Michelle K Mattson-Hoss
Sanford Burnham Prebys Medical Discovery …
7 PUBLICATIONS 67 CITATIONS

SEE PROFILE

Steven P Gross
University of California, Irvine
97 PUBLICATIONS 5,973 CITATIONS

SEE PROFILE

Article

Calibration of Optical Tweezers for In Vivo Force Measurements: How do Different Approaches Compare?

Yonggun Jun,[1] Suvranta K. Tripathy,[1] Babu R. J. Narayanareddy,[1] Michelle K. Mattson-Hoss,[1] and Steven P. Gross[1,*]
[1]Department of Developmental and Cell Biology, University of California-Irvine, Irvine, California

ABSTRACT   There is significant interest in quantifying force production inside cells, but since conditions in vivo are less well controlled than those in vitro, in vivo measurements are challenging. In particular, the in vivo environment may vary locally as far as its optical properties, and the organelles manipulated by the optical trap frequently vary in size and shape. Several methods have been proposed to overcome these difficulties. We evaluate the relative merits of these methods and directly compare two of them, a refractive index matching method, and a light-momentum-change method. Since in vivo forces are frequently relatively high (e.g., can exceed 15 pN for lipid droplets), a high-power laser is employed. We discover that this high-powered trap induces local temperature changes, and we develop an approach to compensate for uncertainties in the magnitude of applied force due to such temperature variations.

INTRODUCTION

First developed by Askin (1), optical tweezers/optical traps (OTs) are a useful tool for manipulating microscopic objects using light pressure. Because of their noninvasive probing of pico-Newton forces, and nanometer-level spatial resolution, they have been widely used in many scientific fields, from single-molecule biophysics to nonequilibrium thermal physics. For example, the force generated by kinesin (2), dynein (3), and myosin (4) have been measured in single-molecule biophysics experiments, where typically a single molecular motor is attached to a bead (handle), which is manipulated by the trap. In physics, OTs have been applied to demonstrate a basic fluctuation theorem, using an RNA hairpin pulling experiment (5), and a basic principle of Landauer's limit for memory erasure was also studied (6).

Recently, efforts have been underway to use OTs to quantify force production in vivo. The first such use was to estimate the typical maximal force available to move mitochondria by measuring the number of mitochondria that escaped from OTs of different strength (7). However, determining the actual force being locally applied in vivo with reasonable accuracy is challenging, and several problems must be overcome. First, local properties of the cytoplasm, such as the refractive index, are unknown, and differences between the refractive index of the trapped object and the surrounding medium contribute to the overall force applied by the trap. Second, the sizes and shapes of trapped organelles vary, sometimes dynamically, which can change the force applied by the OT. Third, due to viscoelasticity of cytoplasm, trapped biomolecules may show

unexpected motion inconsistent with simple diffusion (8), which can make in-cytoplasm calibration efforts difficult. To overcome these difficulties, multiple approaches have been proposed: a refractive index matching method (9,10), a microrheology method (11,12), and a light-momentum-change method (13–16).

The first method—based on refractive index matching—is intuitive and straightforward (9,10). Here, one considers the fact that the force applied by the OT is sensitive to the size of the trapped object but also to the difference in the indices of refraction between the trapped object and the surrounding medium. Thus, one assumes that the stiffness of the OT in cells can be obtained from prior calibration of the force applied to a bead in solution in vitro, once the bead is in a solution such that the difference between the refractive indices of the bead and the solution is the same as that between the refractive indices of the cargo and the cytoplasm. To this end, the average cytosolic index of refraction was measured. Then, to avoid difficulty in calibration from viscoelastic properties of the cytoplasm, the cargo (in this case lipid droplets (LDs)) was purified away from the cytoplasm and suspended in a Newtonian index-matching solution, for example, a 20% sucrose solution. The size of LDs and the stiffness of the trap were determined in this index-matching solution with a conventional power-spectrum method. Once the trap stiffness, K_{OT}, for the specific conditions studied has been determined, the instantaneous force applied by the trap is determined by multiplying the displacement of the trapped object from the trap center by the trap stiffness, i.e., $F = -K_{OT}x$. The displacement, x, is usually measured directly, either from the deflection of the laser beam, or from video imaging. This method is easy to implement, but has limitations: it

does not consider local variations in the cytoplasmic index of refraction, and cannot accurately probe force if the trapped organelles are both nonuniform, or nonspherical, and also not always free to rotate in the OT (see Discussion).

The second method includes consideration of the microrheology of the cytoplasm, which may be non-Newtonian (11,12). Here, an introduced cargo is sinusoidally perturbed using a piezoelectric stage or acoustooptic device, and its motion is recorded to obtain a power spectrum of fluctuations; this is done at different positions in cells. The stiffness of the OT, as well as the viscoelastic moduli, can then be determined by fitting the local experimentally measured power spectra with theoretical equations. This method addresses variations in the local viscoelasticity of the cytoplasm and allows one to probe the force of the object once that local viscoelasticity is calibrated, but to the extent that the object moves away from the location of calibration, such local information is lost. Despite these advantages, there are significant disadvantages as well. First, it is complicated to implement and requires a calibration process for each object before real measurement can take place. Second, it assumes that the local variations are static—if they change over time, it will be wrong. Finally, it also cannot easily address the case of nonuniform objects that dynamically change shape, or even nonchanging nonuniform objects, unless they are free to rotate in the trap (see Discussion). For these reasons, we have not pursued it. Instead, we compare the index-matching approach—which has the benefit of extreme simplicity—with the light-momentum-change method, which nicely complements this microrheology approach (see Discussion) and is easier to implement.

The light-momentum-change method was originally proposed by Smith et al. (13), who used a dual-beam OT, and was subsequently developed by Farré et al. (14) for use with a single-beam OT. The basic idea is to measure the momentum change of the scattered light. Since the change in momentum is caused by the applied force, if one can capture all of the scattered light, and there are no additional scattering centers other than the trapped object, one directly measures the force that the trap applies without needing to know any details about the trapped object, including its size or shape, or the local properties of the medium surrounding the trapped object. This approach thus does not directly involve measurement of the displacement of the cargo relative to the trap center. In principle, this method is ideal for in vivo measurements, though only if the sample is relatively thin, so that all of the laser light can be captured. In practice, to use the light-momentum-change method in vivo, one must first calibrate the system (likely in vitro), which is typically done relative to an existing method under ideal conditions. Thus, the extent to which the initial non-momentum-change trap is correctly calibrated will determine the ultimate accuracy of the momentum-change measurements. During the course of

our studies, we realized that various factors contribute to errors in the more standard calibration approaches, even in vitro, so we first address these and later discuss implementation of the momentum-change approach.

MATERIALS AND METHODS

Setup

The OT used in the experiment was built based on an inverted microscope (TE200, Nikon, Tokyo, Japan) with a trapping laser system (see Fig. 1). A 980 nm near-infrared diode laser (up to 500 mW; EM4, Bedford, MA) coupled to an optical fiber is used for optical trapping. The laser power used was sufficiently high to trap small organelles inside the cell, typically up to 200 mW in the sample. The 980 nm laser was selected to reduce optical damage to the cells (17) and because high-power 980 nm diode lasers are more available than similar 830 nm lasers. The optical fiber of the laser is connected to a collimator (PAF-X-7-B, Thorlabs, Newton, NJ), which is used for alignment, to obtain a laser beam of minimum divergence. The collimated beam is expanded with one concave lens (L1) and one convex lens (L2) and steered with two convex lenses (L3 and L4). The beam is focused by a 100× oil immersion objective (NA 1.3) close to the bottom of the sample chamber. The sample chamber is placed on the *xyz* piezoelectric stage (P-517.3CL, Physik Instrumente, Karlsruhe, Germany), which is installed in the microscope. The scattered beam is collected by the oil-immersion infinity-corrected condenser (NA 1.4).

To achieve high temporal and spatial resolution, the position of the bead or cargo is measured with back-focal-plane interferometry (18). The interference pattern between unscattered and forward-scattered light on the back focal plane of the condenser is used to determine the lateral position of the trapped bead. The conjugate image of this pattern is projected onto the position-sensitive diode (PSD) (DL100-7-PCBA3, Pacific Silicon Sensor, Thousand Oaks, CA). Later, back-focal-plane interferometry is adapted to directly measure force exerted by the OT through momentum change (15). The signal acquired from the PSD is sent through a data acquisition device (PCI-6229, National Instruments, Austin, TX) to the computer and analyzed by a custom LabVIEW program.

The mercury lamp is mounted above the condenser for bright-field imaging. The charge-coupled device (CCD) camera (30 fps, Dage-MTI-100, Michigan City, IN) is placed on the image plane and is used to monitor
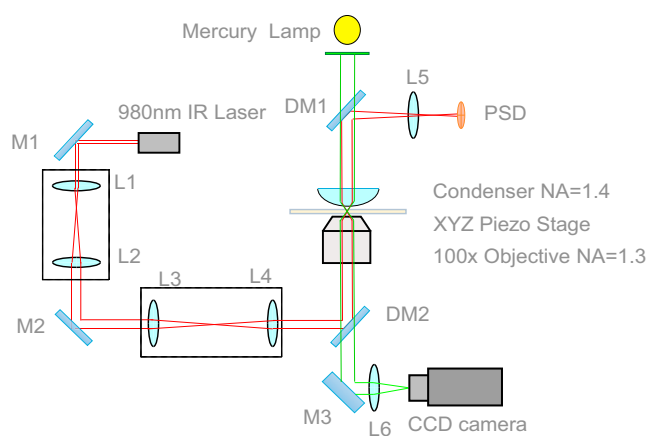

FIGURE 1   Schematic of the OT setup. A 980 nm infrared laser is used to trap a nanosize bead. The beam is expanded with lenses L1 and L2 and steered by lenses L3 and L4. The bead in the sample cell is monitored by CCD camera, and its motion is recorded by PSD of 3 kHz. The *xyz* piezo stage is used to obtain the conversion coefficient (β, nm/V). To see this figure in color, go online.

and record images analyzed in real time to track the position of a bead of interest. The tracking software is written with LabVIEW and a built-in template-matching algorithm and has been previously described (19).

Passive power-spectrum method

The passive power-spectrum method is the most common way to calibrate a trap (20,21) and is usually considered to be the most reliable, since analysis in the frequency domain provides information about different sources of noise, which can either be discarded when doing the fitting or eliminated from the experiment if possible. When a submicron-size bead is trapped by the OT in solution, inertial effects are irrelevant, and viscosity is dominant. The motion of a trapped bead is then described using the overdamped Langevin equation,

$$K_{OT}x + \Gamma\dot{x} = \xi(t), \tag{1}$$

where K_{OT} is the stiffness of the trap, $\Gamma = 6\pi\eta r$ is the bead drag coefficient, and $\xi(t)$ is the Langevin force, which obeys $\xi(t) = 0$ and $\langle\xi(t)\xi(t + \tau)\rangle = 2\Gamma k_B T\delta(\tau)$. Here, η is the dynamic viscosity of the solution, r is the radius of the bead, k_B is the Boltzmann constant, and T is the Kelvin temperature. The power spectrum of position fluctuations of the bead can be obtained by Fourier transform of Eq. 1:

$$G(f) = \frac{2|\hat{x}(f)|^2}{t_{msr}} = \frac{k_B T}{\pi^2\Gamma(f_c^2 + f^2)}, \tag{2}$$

where t_{msr} is the measurement time and f_c is the cutoff frequency.

Based on the assumption that the focused light has little effect on the local temperature, and that therefore the local temperature of the bead is the same as room temperature, we can determine the trap stiffness, K_{OT}, from the power spectrum: $K_{OT} = 2\pi\Gamma f_c$. Note that in addition to assumptions about the temperature, this method requires that the trapped object be spherical and of known radius. Such an assumption may not be true when examining a purified cargo from a cell. For this reason, an equipartition approach has sometimes been employed (see next section).

Equipartition theorem

A molecule in solution moves continuously due to heat. Thermal fluctuations can thus be used to calibrate the stiffness of the OT. Because the OT is assumed to be a harmonic potential, the equipartition theorem is as follows when thermal fluctuations are balanced with harmonic potential:

$$\frac{1}{2}K_{OT}\sigma^2 = \frac{1}{2}k_B T, \tag{3}$$

where σ is the standard deviation of the position, x, of a bead in relation to the center of the trap, k_B is the Boltzmann constant, and T is the absolute temperature. This method makes it possible to determine the stiffness of the trap without knowing details such as the viscosity of the medium and the size or shape of a trapped bead (however, see Discussion for caveats). The temperature, T, is the only parameter needed to determine the stiffness. Although this method thus has advantages over others, it has not been preferred previously, because it is quite sensitive to a variety of noise sources.

Active power-spectrum method

Another calibration method recently proposed by Tolić-Nørrelykke et al. (22) is the active power-spectrum method, which has the advantage of determining both the stiffness and the conversion constant simultaneously. While a bead is trapped in the OTs, the whole sample cell (mounted on the piezoelectric stage) moves sinusoidally with the driving frequency, f_{dr}, and the position of the sample cell, x_{dr}, is

$$x_{dr} = A\sin(2\pi f_{dr}t), \tag{4}$$

where A is the amplitude of sinusoidal perturbation. The Langevin equation is rewritten with the effect of sinusoidal motion of the sample cell:

$$K_{OT}x + \Gamma(\dot{x} - \dot{x}_{dr}) = \xi(t). \tag{5}$$

The corresponding power spectrum is represented with the sum of the power spectrum of the trapped bead due to thermal fluctuations and the sinusoidal stage driving frequency:

$$G(f) = \frac{k_B T}{\pi^2\Gamma(f_c^2 + f^2)} + \frac{A^2}{2\left(1 + f_c^2/f_{dr}^2\right)}\delta(f - f_{dr}). \tag{6}$$

Here, T, A, and f_{dr} are the known parameters, and Γ and f_c can be obtained from fitting to experimental data. The last term is the δ-function spike at the driving frequency.

When the displacement, x, of the bead from the center of the OT is measured, it is determined as a function of voltage (V) from the PSD: $x = \beta V$, where β is the conversion factor to convert from voltage to nanometers. The power spectrum is then represented as

$$G(f) = \beta^2 G_V(f), \tag{7}$$

where $G_V(f)$ is the experimentally obtained power spectrum of the dimension, V^2s^{-1}. The conversion factor is determined as

$$\beta = \sqrt{\frac{W_{th}}{W_{ex}}}, \tag{8}$$

where $W_{th} = A^2/[2(1 + f_c^2/f_{dr}^2)]$ is the theoretical estimated spike and $W_{ex} = [G_V(f_{dr}) - G_V^{back}(f_{dr})]/t_{msr}$ is the experimentally obtained spike. Here, G_V^{back} is the thermal background at the frequency, f_{dr}. From Eq. 7, the drag coefficient, $\Gamma = k_B T/D_V\beta^2$, and the stiffness, $K_{OT} = 2\pi k_B Tf_c/D_V\beta^2$, can be experimentally determined. Here, D_V is the experimentally obtained diffusion constant with dimension V^2s^{-1}.

This active power-spectrum method has several advantages, particularly relative to the assumptions required for the passive power spectrum: 1), it is able to determine K_{OT} and β simultaneously, 2), it does not require prior knowledge of viscosity of the medium, the size of the bead, or the height of the trapped object above the surface; and 3), it is less sensitive to temperature changes. Compared to other calibration methods, this is our method of choice: it is insensitive to system noise, its result inherently includes the output of the passive power-spectrum method, and it allows simultaneous measurement of β and K_{OT}.

Force measurement through momentum change

In the traditional approach (23), the force, F, measured in the OT is proportional to the stiffness of the trap, K_{OT}, and to the relative displacement, x, of the trapped object from the center of the trap. That is, $F = K_{OT}x$, and $x = \beta V$, where β is the conversion constant between the real position and the output voltage, V, of the PSD. By calibrating the quantities K_{OT} and β, we can then precisely determine the force exerted by the OT.

As indicated in the Introduction, another approach is to measure force directly, by determining the change in light momentum between incident and scattered laser light (15). When the light beam interacts with the trapped object, the beam is diffracted at angle θ. When all scattered light is collected on a detector such as the PSD, the momentum change, dp, is $(nW/c)dt$, where W is the laser power and n is the refractive index of the medium, c is light velocity, and dt is the time change. The force exerted by the OT on a cargo, then, is measured by means of time-dependent lateral momentum change between the bead and the laser beam, as

$$F_x = -\frac{dp}{dt} = \frac{nW}{c}\sin\theta = \frac{R_D}{\psi f' c}V_x \equiv \alpha V_x, \qquad (9)$$

where R_D is the detector size, ψ is the conversion between watts at the sample plane and volts from the detector, and f' is the focal length of the condenser (see Farré et al. (15) for a more detailed theoretical description). Using the previous calibration from the power-spectrum method, we then have

$$F_x = K_{OT}\,x = K_{OT}\,\beta V_x = \alpha V_x. \qquad (10)$$

The last equivalence is from Eq. 9. Critically, force constant α can thus be determined from β and K_{OT}, and it is independent of bead size, bead shape, laser power, and the refractive index of the bead and medium. Thus, α can be determined in vitro, and then used for in vivo measurements. Because α is directly determined as a a function of β and K_{OT}, errors in the latter parameters will ultimately impact the reliability of α.

In vitro kinesin motility bead assay

Kinesin was purified from bacteria as previously described (24). Kinesin was incubated with carboxylated polystyrene beads (490 nm, Polysciences, Warrington, PA), 1 mM ATP, and an oxygen-scavenging system (250 μg/mL glucose oxidase, 30 μg/mL catalase, and 4.5 mg/mL glucose) in 50 μL bead motility buffer (80 mM PIPES, pH 6.9, 50 mM CH_3CO_2K, 4 mM $MgSO_4$, 1 mM dithiothreitol, 1 mM EGTA, 10 μM taxol, and 1 mg/mL casein) for 15 min at room temperature. Diluted kinesin was bound to beads to yield binding fractions of <35%. Kinesin-bound beads were flowed into flow cells with taxol-stabilized microtubules, and all measurements were performed at $T = 24°C$ in bead motility buffer.

Sample preparation for in vivo measurement

HEK293 cells were grown in DMEM (Invitrogen, Carlsbad, CA) supplemented with 10% fetal bovine serum at 37°C in 5% CO_2. For measurements, cells were plated on poly-L-lysine-coated coverslips and grown for 24–48 h under normal conditions.

RESULTS

Since they are used to determine α, we start by comparing the different approaches to find β and K_{OT} in vitro. Measurements were performed in water, calibrating the trap with both 642 nm silica beads and 490 nm polystyrene beads at room temperature (24°C). The trapping laser was used at different powers, up to a maximum of 200 mW in the sample. The 980 nm laser causes 3.5 times the heating of an equivalently powered 1064 nm laser, and 16.5 times the heating of a similar 830 nm laser, so this in principle may be significant. We applied two corrections for viscosity: temperature (25) and Faxén's law (23). The viscosity of water is a function of temperature and can be calculated based on the equation $\log[\eta(T)] = 0.0023611/T^2 + 0.068922/T - 0.3908$ (25). Nearby surfaces amplify viscous drag, so Faxén's law, with $\Gamma_{Faxén} = 6\pi\eta r/[1 - 9r/16h + r^3/8h^3 - 45r^4/256h^4 - r^5/16h^5 + \cdots]$, was used to correct for this effect. Since the measurements were made 3 μm above the surface, the Faxén's corrections were 5.7% and 5.2% for 642 nm silica beads and 490 nm polystyrene beads, respec-

tively. Here, r is the radius of a bead and h is the distance from the surface to the center of a bead.

Below, we first determine the conversion constant, β, and the stiffness, K_{OT}. After evaluating which procedure was most appropriate, we then use these to determine the force constant, α, for the momentum-change approach.

Estimation of the conversion constant, β

We first use the active power-spectrum method to calibrate β. The piezoelectric stage was sinusoidally displaced with $f_{dr} = 50$ Hz and $A = 72$ nm. We obtained the 50 trajectories ($t_{msr} = 1$ s each) at 44 kHz to calculate the power spectrum and averaged all power spectra to reduce noise. One sample of such a power spectrum is shown in Fig. 2 a. W_{ex} is obtained from the difference between the peak and base values at 50 Hz and f_c from Lorentzian fitting using Eq. 2. To make sure this method gives an accurate β, we used kinesin motion to generate additional motion of the bead relative to the OT. We could then also obtain β directly by monitoring the motion of a bead (Fig. 2 b) with video as well as the OT. Specifically, when the bead was trapped by the OT at a given laser power, its trajectories (caused by binding and walking of kinesin) were recorded simultaneously with
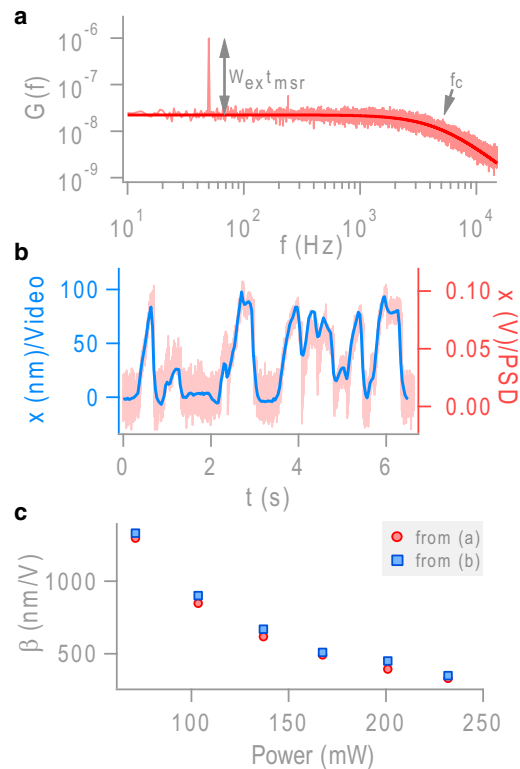

FIGURE 2 Estimation of the conversion constant, β. (a) Power spectrum at $f_{dr} = 50$ Hz. (b) Kinesin method: trajectories of a bead moved by kinesin, obtained from the CCD (left vertical axis) and the PSD (right vertical axis). (c) Comparison between β as a function of input laser power obtained from a and that obtained from b. To see this figure in color, go online.

the CCD camera (30 Hz) and the PSD (3 kHz). The conversion constant from nanometers to pixels for the CCD is 30 nm/pixel, independent of the trapping laser power, and we can determine the position of the bead with few-nanometer resolution by means of particle tracking and analysis (19). The conversion constant, β, can then be verified by comparing the voltage from the PSD to the nanometer value obtained from the CCD image. Note that instead of using kinesin to move the bead, for those outside of the motor field, the same effect as seen in Fig. 2 b could be obtained by using a bead tethered to the microscope slide and displacing the slide by different amounts laterally using a Piezo-controlled stage. Because viscosity does not contribute to determination of β, in the latter approach, the measurements were made close to the surface. Fig. 2 c shows the summary of β determined for different laser powers, with quantitative agreement between the two methods. The two curves collapse on each other and are fit well with the inverse of power, as expected since K_{OT} is linearly proportional to power. Thus, the active power-spectrum method is an easy and reliable way to determine β.

Calibration of stiffness

In the Introduction, we indicated that multiple calibration approaches have been used in vitro. Here, to obtain the OT stiffness, we directly compare three of these approaches: equipartition theorem, and the passive and active power-spectrum methods. Fig. 3 (upper) shows the time series of

fluctuations of the bead position without external perturbation (Fig. 3 a) and the corresponding histograms for three different laser powers (Fig. 3 b). Based on the assumption of a harmonic potential, the distribution of x must obey the Boltzmann distribution in the equilibrium state: $P(x) = P_0 \exp[-U(x)/k_B T]$ and is well fitted by a Gaussian distribution. For the OT, $U(x) = K_{OT} x^2$. Fig. 3 c represents the active power spectrum of bead position fluctuations with external perturbation. We calculated 50 sets of power spectrum with 1 s time series and averaged them. One way to determine K_{OT} (the passive power-spectrum method) is by Lorentzian fitting of the power spectrum (23) to obtain the cutoff frequency, f_c, that corresponds to $K_{OT}/2\pi\Gamma$. An alternative approach is the active power spectrum method, $K_{OT} = 2\pi k_B T f_c / D_V \beta^2$.

Fig. 3 d summarizes the trap stiffness, K_{OT}, as a function of power for the three approaches. We found that K_{OT} values determined by both the equipartition theorem and the active power-spectrum method are close to each other (triangles and circles), whereas K_{OT} determined by the passive power-spectrum method (squares) not only is larger than the others, but is also a convex function of laser power, suggesting that the stiffness may be overestimated at higher laser power because it should be a linearly increasing function of power (Eq. 9). We were surprised by the difference between K_{OT} values determined by the passive power-spectrum method and those determined by the other two approaches, and felt that this was worth examining, especially since the former approach appears to be an outlier and yet is widely used.

Temperature effect

In Fig. 3 d, K_{OT} determined by the passive power-spectrum method is quite different from that determined by the other two approaches, and it also changes differently as a function of laser power. Obviously, this is nonphysical: $F = K_{OT} x$, and $x = \beta V$, and the β values for the different methods are the same (Fig. 2), so different K_{OT} values imply different applied forces for the same laser power under the same conditions. The difference between the approaches suggests that there must be a wrong assumption in at least some of the calculations. It is important, too, that in the equipartition and active power-spectrum approaches, trap stiffness does not depend on viscosity, whereas in the passive power spectrum approach, it depends linearly on viscosity.

In principle, the divergence in results using the three approaches might therefore reflect effects of local heating (due to the laser beam) on the viscosity of the medium coupled with differences in treatment of the relationship between trap stiffness and viscosity of the medium. We therefore considered the possibility that the local temperature increased significantly as the laser power increased (26), and we tried to compensate computationally for such a heating effect. To do this, we provided an estimated temperature,

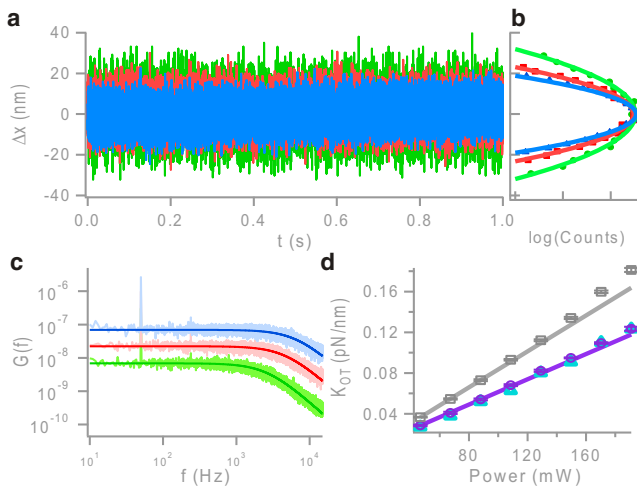FIGURE 3 (a) Trajectories of a 642 nm silica bead trapped in the OT for 67 mW (green), 108 mW (red), and 129 mW (blue) of laser power without external perturbation. (b) Histograms of the trajectories shown in a, which are well fitted with Gaussian distribution. (c) Power spectra based on trajectories with external perturbation, from which K_{OT} can be obtained via the passive and active power-spectrum methods. For presentation, the three spectra (green, red, and blue) were vertically adjusted, although they overlap at lower frequencies. (d) Stiffness of the OT from the equipartition theorem method (triangles), passive power spectrum method (squares), and active power spectrum method (circles) for a 642 nm silica bead. Solid lines are the fit of the first three points, to show how much K_{OT} deviates at high power. To see this figure in color, go online.

T. Since the passive and active power-spectrum methods are performed simultaneously (Fig. 3 d, *squares* and *circles*), they must produce the same experimental output in terms of the stiffness of the trap.

Because viscosity is a function of temperature, we adopt temperature as a control parameter to adjust the stiffness of the trap. For the active power-spectrum method, we can calculate viscosity by using $\eta(T) = k_B T / 6\pi r D_V \beta^2$, where D_V and β are experimentally determined. For the passive power-spectrum method, the effect of temperature on viscosity was calculated from $\log[\eta(T)] = 0.0023611/T^2 + 0.068922/T - 0.3908$ (25). When the variable, T, in the two equations was tuned, the resulting water viscosity estimates gradually approached each other, finally becoming the same at a certain temperature, which we call the estimated local temperature. It can be seen in Fig. 4 a that this value increases monotonically as a function of laser intensity. From our measurement, the temperature increase due to local heating is $\Delta T = 7.8°C/100$ mW for the 490 nm polystyrene bead and $3.8°C/100$ mW for the 642 nm silica bead. This is similar to our predicted rise of $5.1°C/100$ mW (17) and consistent with the experimental results of Mao et al. (27).

Although the biggest adjustment comes from correcting the passive power-spectrum approach by using the estimated temperature to calculate effective viscosity, we note that both of the other methods directly include T in calculation of trap stiffness. Therefore, for consistency, we used the new, estimated T to calculate stiffness in these approaches
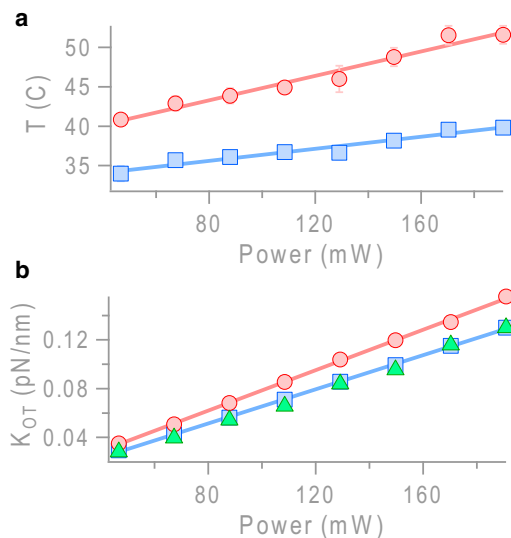
as well (Fig. 4). Fig. 4 b shows K_{OT} after correction for the local temperature effect for 490 nm polystyrene beads (*circles*) and 642 nm silica beads (*squares*), showing that trap stiffness is now a linearly increasing function of laser power. K_{OT} values determined by the active and passive power-spectrum methods now collapse onto a single plot, and K_{OT} determined by the equipartition method (after local temperature correction) (*triangles*) also quantitatively agrees with that determined by the other approaches. Although all stiffnesses were thus corrected, it is important to note that the magnitude of correction for both the equipartition and active power-spectrum approaches was very small, because the stiffness depended linearly on temperature (in Kelvin), and since the (estimated) temperature changed from ~300 K to ~310 K, there was an ~3% correction in stiffness. In contrast, adjusting η decreased the estimated stiffness by 30% or more.

Momentum-change measurements: determining the force constant, α

The force constant, α, is the proportionality constant between the measured voltage change (due to deflection of the light) from the PSD and the overall applied force, and it should thus be independent of bead size and the refractive index of the surrounding media. α can be determined from β (Fig. 2 c) and K_{OT} (Fig. 4 b). We examined three different conditions: 490 nm polystyrene beads in water, 642 nm silica beads in water, and 642 nm silica beads in a 20% sucrose solution. For convenience, we plot K_{OT} as a function of $1/\beta$; the slope is α. As shown in Fig. 5, the three graphs collapse onto a single line, demonstrating that α is indeed a constant value, as assumed. Critically, these data directly demonstrate that α is insensitive to changes in the index of refraction of the surrounding medium, since the refractive index of the 20% sucrose solution is quite different from that of water and close to that of the cytosol (28). In conclusion, we believe that the unaccounted-for variable contributing to
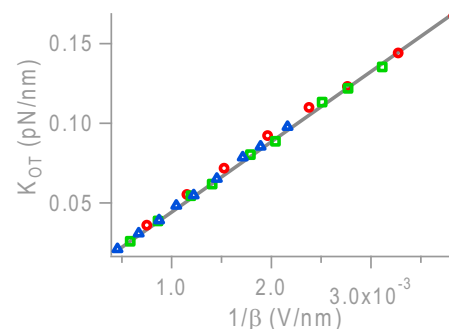
FIGURE 4   Calculated local temperature at the focus of the trapping laser for room temperature of 24°C. Temperature increases 7.8°C/100 mW for a 490 nm polystyrene bead (*red circles*) and 3.8°C/100 mW for a 642 nm silica bead (*blue squares*) in water. (b) Stiffness of the OT after correction for the local temperature effect, for a 490 nm polystyrene bead (*red circles*) and a 642 nm silica bead (*blue square*s). Green triangles represent the stiffness for a 642 nm silica bead as determined using the equipartion-theorem method after temperature correction. To see this figure in color, go online.

FIGURE 5   Force constant α determined from measurements of a 642 nm silica bead in water (*green squares*) and in 20% sucrose solution (*blue triangles*), and a 490 nm polystyrene bead in water (*red circles*). This is a re-plot of K_{OT} (Fig. 4 b) versus $1/\beta$ (Fig. 2 c) to get α. All curves collapse each other and the slope, α, is 44 pN/V. To see this figure in color, go online.

the difference in results using the distinct calibration methods was the influence of laser power on local temperature, and hence on viscosity. Once we correct for this variable, the different methods agree.

Force measurement in vitro

To objectively confirm that our temperature-corrected viscosity approach yields the correct result, we applied a known force to beads, and confirmed that each method gave the same result. To do this, we took advantage of kinesin, a homodimeric motor that walks along microtubules with 8 nm steps using energy from ATP hydrolysis (2), because it functioned robustly in our previous study (29) and has a well-defined stalling force. Here, we attached a single motor to different-sized beads and in each case determined the stall force of kinesin. The bead assay was carried out as in a previous experiment (24), in which recombinant kinesins were tethered to carboxylated polystyrene beads (see Materials and Methods). The bead, secured in the OT, was moved to just above a microtubule immobilized on a polylysine-coated coverslip. When the kinesin bound to the microtubule, it walked toward the plus end. Since the OT exerts an opposite force, kinesin eventually stops moving.

Kinesin stall forces were measured using three different laser intensities (Fig. 6 a). Using β and temperature-corrected K_{OT}, we see that the stall force is not a function of laser power (red circles), as expected. Also shown are stall forces as they would be determined from the non-temperature-corrected active (green triangles) and passive (blue squares) power-spectrum methods; the uncorrected passive power-spectrum approach shows a nonphysical relationship between stall force and laser power. We note that past reports of the kinesin stall force vary from 4 to 7 pN (30–34), and Fig. 6 a suggests that much of this variation might be due to differences in calibration combined with differences in heating due to the use of different lasers and trapping laser power.

To test the validity of the light-momentum-change method, we measured kinesin stall forces with three different sizes of polystyrene bead: 489 nm, 789 nm, and 981 nm (Fig. 6 b) at 100 mW laser power. Here, the same (fixed) α was used. We note that because the trap stiffness is a function of bead size, the actual trap stiffness in each case was quite different: 0.05 pN/nm, 0.07 pN/nm, and 0.1 pN/nm for the three sizes, respectively. Thus, the stalling distance from the center of the trap varied according to bead size, but the output voltages from the PSD reflecting the overall momentum change in the light were the same, indicating that the stall forces were the same. This directly confirmed that using the momentum-change method, it is not necessary to have a priori knowledge—or accurate determination—of the size of the trapped object.
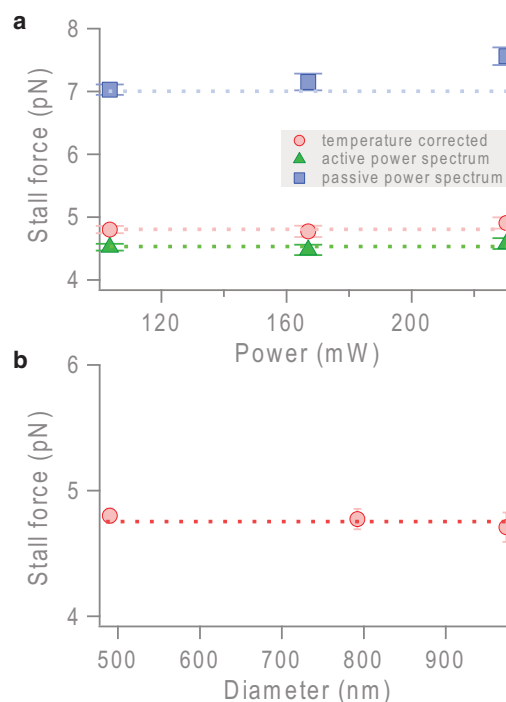

FIGURE 6 (a) Kinesin stall forces determined by three different calibration methods: passive (blue squares) and active (green triangles) power-spectrum methods and the temperature-correction method (red circles). The stall force for the passive power-spectrum method increases according to trapping laser power, indicating that K_{OT} is overestimated. (b) The stall force for kinesin determined from the momentum-change method, using fixed α, with three different-sized polystyrene beads with diameters of 489 nm, 789 nm, and 981 nm. They show the same stall force at the laser power 100 mW. To see this figure in color, go online.

Force measurements in vivo

We confirmed above that the momentum-change method is an effective way to determine the force applied by the OT, that it gives the same result as the trap stiffness/displacement approach, and that it is insensitive to the actual size of the cargo (Figs. 5 and 6) and the local index of refraction of the surrounding medium (Fig. 5). We now apply this in vivo.

Calibration of bead size and stiffness of the trap for the refractive index matching technique

The size of LDs varies in cells and is difficult to determine in real time. Because cargo size affects trap stiffness, determination of the exact size of the LD is necessary for in vivo force measurements using the K_{OT} method. One way to estimate LD size is the refractive index matching technique. Silica beads immersed in water were used to determine the size of the LD, because the difference in refractive index between water and a silica bead is very close to that between cytosol (n = 1.355) and an LD (n = 1.465) (9). One visual example is the DIC images of an 530 nm silica bead in water (Fig. 7 a, upper) and an ~530 nm LD in HEK293 cytosol (Fig. 7 a, lower). To find the ratio of real size (nm) to pixel
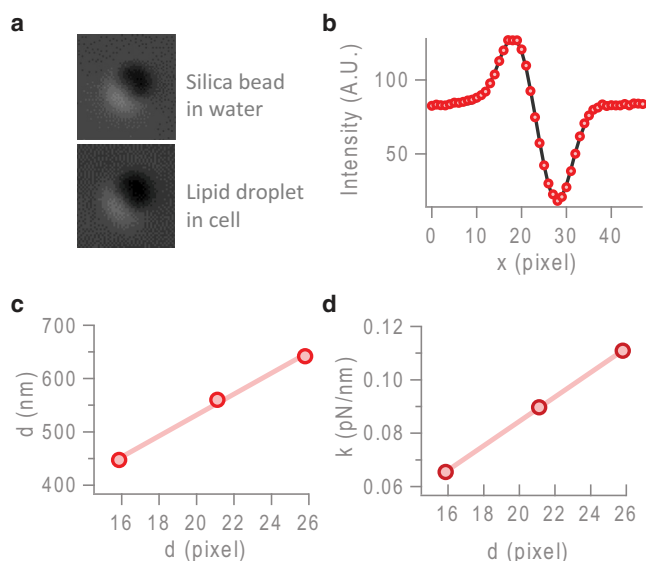
FIGURE 7 (a) Images of a silica bead in water (*upper*) and an LD in a cell (*lower*). (b) Intensity profile of the bead and two-Gaussian fit. (c) The stiffness of the silica beads for a laser power of 170 mW and the bead size in real units versus pixels. (d) Ratio of the force from the index-matching technique to that from the momentum-change method. To see this figure in color, go online.

size, the DIC image was rotated 45° and the intensity profile of the bead was drawn across the center of the bead. To determine the size, the intensity profile was fit with the sum of double Gaussian functions as shown in Fig. 7 b: $I(x) = I_O + A_1 e^{-(x-x_1)^2/\sigma_1^2} - A_2 e^{-(x-x_2)^2/\sigma_2^2}$, where I_O is the background intensity of the image and x_1 (x_2) and σ_1^2 (σ_2^2) are the center and variance of the bright (dark) area. From this, the diameter of a bead was calculated as $d = |x_2 - x_1| + \sigma_1 + \sigma_2$. Fig. 7 c shows that the size of silica beads of known diameter in pixels is proportional to the actual bead size in nanometers. Average sizes of silica beads were obtained from 25 different measurements with three different silica bead sizes, 447 nm, 516 nm, and 642 nm. The stiffness of the trap, calculated based on the average of 10 trials, also shows a linear relationship with bead size, as in Fig. 7 d. For all measurements, the power of the laser was fixed at 170 mW and beads were trapped at 3 μm above the surface of the coverslip. A calibration curve of the apparent size as a function of the real size was constructed and used to determine the real size of individual LDs.

Actual force measurements

To compare the index-matching and light-momentum-change methods, we used both measurement approaches in HEK293 cells. When a linearly moving LD was detected, the trapping laser was initially off, and the piezo-electric stage was used to move the sample so that the center of the LD was positioned at the center of the trap. The trapping laser was then turned on. To compare forces determined

using the two different approaches, we recorded video images and acquired the signal from the PSD simultaneously.

Small LDs (<450 nm) typically escaped rapidly after being exposed to the OT, since the maximum trap force applied to these LDs was smaller than the pulling force of the molecular motors attached to them. In contrast, larger LDs (500–700 nm) could generally be trapped, and they showed either true stalls or repeated attempts at stalling as the LD tried to escape the trap, detached, returned to the center of the trap, and tried again. Fig. 8 a shows a typical force trajectory for LD motion. The blue line (larger values) represents the force calculated by the index-matching method, F_{im}, and the red line (smaller values) the force calculated by the momentum-change technique, F_{mc}. We repeated the experiments multiple times on different LDs and in different cells and obtained the F_{im}/F_{mc} ratio
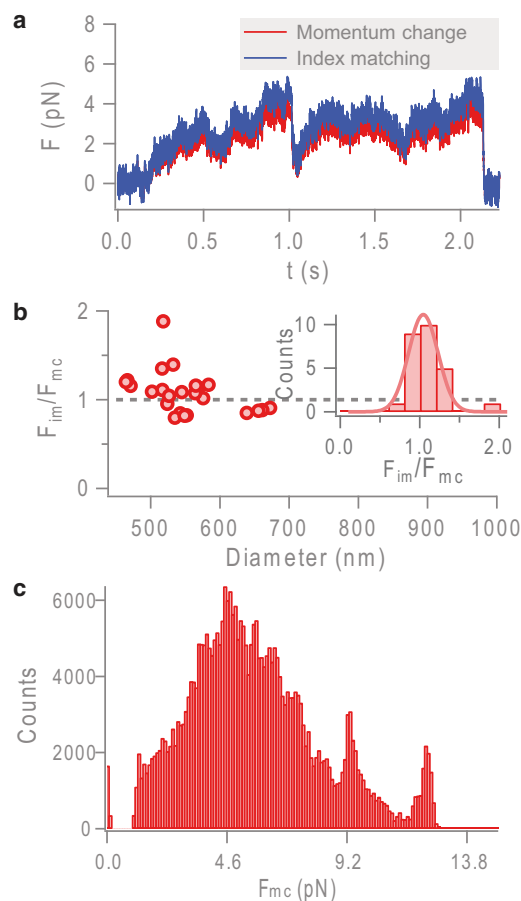

FIGURE 8 (a) Force measurement by the index-matching method (F_{im}) and the momentum-change method (F_{mc}). The force trace is acquired at 3 kHz. (b) Comparison between two force measurements. The ratio of F_{im} to F_{mc} is plotted as a function of the diameter of the LDs. The average of the ratio is 1.08. (*Inset*) Histogram of F_{im}/F_{mc} and the Gaussian curve. (c) The histogram of force generated by kinesin in a Hek293 cell measured by the momentum-change method, which is the sum of 94 force trajectories (for instance, F_{mc} in a). The peaks are at 4.6 pN and 9.2 pN. To see this figure in color, go online.

(Fig. 8 b). F_{im}/F_{mc} was normally distributed around 1 (Fig. 8 b, inset), with an average of $F_{im}/F_{mc} \sim 1.08$, indicating that the two methods give essentially the same estimate of force.

Kinesin moves in the plus-end direction, which here is toward the periphery of the cells. In this case, although we are not certain that these LDs are moved by kinesin-1 (Kin-1), it is very likely, based on reports in the literature that Kin-1 moves LDs in *Drosophila* embryos (35) and, more recently, that Kin-1 moves LDs in mammalian Cos-1 cells (unpublished data, S.P. Gross, B.R.J. Narayanar- eddy), where anti-Kin-1 RNAi causes complete loss of LD motion. If LDs are not moved by Kin-1, the most likely agents of movement are Kin-2 or Kin-3, which are reported to have stalling forces similar to that of Kin-1 in vitro (36,37). We thus measured the actual distribution of plus- end-driven LD forces in HEK293 cells. Histograms were obtained from each force trajectory of kinesin-driven motion inside the OT, and all the histograms were summed (Fig. 8 c); this histogram reflects measurements from N = 94 LD trajectories. Previous studies show different apparent unitary forces in different cell lines, for example, ~4 pN from LD movement in A549 human lung cancer cells (10), 2.6 pN from LDs moving in *Drosophila* embryos (9), 5.8 pN from the motion of latex beads phagocytosed into J774.2 cells (32), and 6 pN from the motion of latex beads phagocytosed into mouse macrophage cells (11). We were intrigued to find that in contrast to some other mea- surements in other cell types, peaks here were observed at 4.65 pN and 9.25 pN. This would be consistent with the ~4.8 pN in vitro measurement shown in Fig. 6. Another peak at 12.2 pN in Fig. 8 c is the upper limit of force measurement under in vivo conditions in our setup, and would be consistent with three kinesin motors functioning together, since kinesin forces in vitro are slightly subaddi- tive (33). Nonetheless, other work suggests that deformation of flexible cargos may alter the way motor forces add (38), suggesting caution in relating the measured force to a spe- cific number of motors. Exactly how forces vary between different cargos and cell types will be a fruitful area for future study.

DISSCUSSION

With the ultimate goal of making well-calibrated force mea- surements in vivo, we compared three different calibration methods. Ultimately, we favor the momentum-change approach, which is easier to implement in the sense that cali- bration (to determine α) is a one-time event, and once cali- bration is completed, the method is insensitive to multiple unknowns, such as cargo size variation, local changes in cytosolic refractive index, etc. Although this is true, the average difference between the momentum-force measure- ments and the index-matching approach nonetheless ap- pears to be rather small (Fig. 8 b), so the in-principle insensitivity to such effects may in practice not be impor-

tant. Our data suggest that either approach will work, at least for LDs that tend to be spherical and do not change shape dramatically, and under the conditions we used, where the cell is likely not making significant dynamic changes to the cytosol.

However, under some conditions, it is easy to imagine different methods diverging. First, under some stimuli, the cytoskeleton can rapidly rearrange (e.g., within ~30 s to 1 min for actin (39)), and in such cases, the local cytosolic viscosity and perhaps even the local index of refraction could change significantly. Methods that either assume a uniform refractive index (such as the index-matching approach) or assume that viscosity and refraction index are locally fixed (such as the microrheology methods that first calibrate trap stiffness at different cellular locations and then use these values) may be prone to unexpected errors in such situations. In a similar way, cargos can un- dergo shape changes. For instance, typical mitochondria frequently elongate or deform dynamically. Any calibration that is done at a single point in time, when the mitochondria have a particular shape, for example, will likely be less accurate later, as the cargo shape changes.

One important difference between in vitro and in vivo measurements is that the environment is typically isotropic in vitro, whereas this may not be the case in vivo. To the extent that the isotropic assumption fails, the active calibra- tion (microrheology) approach may not be correct: perturba- tions are driven in specific directions, and if, for example, the molecular motors move the cargo in different directions, the local opposition to motion in a given direction may be different from opposition to motion in the direction origi- nally tested. Similar issues are true for cargos of fixed irreg- ular shape: in solution, these objects are free to rotate, and so will tend to sit in the OT in a particular rotation; the deter- mination of trap stiffness, once made, should be accurate as long as the cargo doesn't change shape. However, in vivo, local constraints (multiple actin filaments or multiple attach- ments to a microtubule) may prevent a cargo from rotating. In such cases, the orientation of the cargo in the OT may be different from the original calibration, and to the extent that this occurs, the calibrated trap stiffness may be incorrect. All of these issues are avoided by using the momentum- change approach, where both the force applied by the OT and the direction of this force are simultaneously measured by how the momentum of the light changes.

Nonetheless, the microrheology (active) approach is im- portant, because it provides information not provided by the momentum-change method. It is frequently the case that we want to understand not only the maximum possible force exerted by the motors, but also how much opposition they encounter. The force measured by the momentum- change approach is the difference between the maximum force the motors can apply and the force opposing their motion (e.g., due to viscoelastic properties of the cytosol). As such, to the extent that other forces oppose the motion

of the cargo, the force measured by the momentum-change approach will underestimate the actual maximum possible force of the motors. In contrast, the active approach provides knowledge of the local cytoplasmic properties, allowing additional insight. It is thus an important complement to the momentum-change approach, and it may prove valuable to apply these methods in conjunction.

Although the momentum-change method has many advantages, it does require specific conditions (15) to function. All the scattered light must be gathered, and one must use a very high-NA (~1.4) condenser to achieve this. Also, a relatively low-NA objective (~1.3) is preferable, because the input cone of light is then narrower, making it easier for the high-NA condenser to gather all scattered light. The use of the 1.3 NA objective (rather than the 1.4 or 1.5 NA objective traditionally preferred for optical trapping) means that for a given laser power, the OT is a bit weaker. Further, this approach cannot be used in a thick sample chamber (<100 μm), since then some of the scattered light is not captured. Although it has been suggested that measurements should be made with the sample positioned within 30 μm of the upper surface of a sample chamber (15), we find that the method works as long as we are within ~50 μm. Empirically, we always monitored the sum signal to confirm that most of the scattered light was collected, and we found the loss of the light to be $<5\%$. Although quadrant photodiodes (QPDs) might appear more sensitive, one must use a PSD instead a QPD, because the output of the QPDs is sensitive to sample size, and not merely to location of the centroid of light (15).

Another limitation of the momentum-change method is that using the PSD signal to determine the position of the trapped object is not straightforward. Although one records the voltage signal, and thus has the same raw data as in the index-matching approach, to interpret the signal (i.e., to use the signal from the deflected beam to infer the position of the trapped object that scattered the beam), one must know β (the relationship between the displacement of the object and the amount the light is scattered). As discussed above, β depends on multiple factors. Without a β value appropriate for the specific cargo in the trap, the scattered signal cannot be used to extract the position of the trapped object. In our case, we use a two-step approach. We start by directly measuring the position using video (particle tracking). This correctly yields position, but with somewhat limited temporal resolution (30 fps). For data with higher temporal resolution (>1 kHz), we must determine β for the cargo of interest from the PSD. To do so, we take advantage of the fact that $x = \beta V$, where x is the position (determined from video), β is unknown, and V is the voltage from the PSD. Then, β is simply determined via fitting, by finding the multiplicative factor required to match the V signal to the x signal (see Fig. 2 b). Critically, β determined by this fitting approach is the same as β determined directly from the active power-spectrum method (Fig. 2 c), giving us confidence in the final result. Once β has been determined for the

specific cargo in question, the PSD signal can be used for position determination with high temporal resolution.

With regard to our investigation of calibration methods, we found that the passive-diffusion calibration approach appears particularly sensitive to temperature-induced changes in viscosity, which can result in significant calibration errors. Since this method is widely used, we believe this observation is important, as is the fact that one can correct for such effects by using a calculated effective temperature to address the effect on viscosity. We acknowledge that for the moment, the estimated effective temperature is essentially a computational correction, and the extent to which it actually reflects a true change in temperature remains to be investigated. However, although the magnitude of the correction is large for the passive power-spectrum approach, it is quite small for the active power-spectrum estimation of trap stiffness favored here and thus does not dramatically affect the accuracy of our in vivo force determination.

We also used the momentum change method to obtain kinesin stall forces from in vitro bead assays and from LDs moving in a living HEK293 cell. The stall forces were ~4.8 pN for single motors in both cases, consistent with previous in vitro measurements (33). This suggests that the momentum-change method is a useful tool for measuring the in vivo force of molecular motors.

We noted above that the momentum-change method determines only how much force is required from the trap to stop the motion of a cargo or a bead, and that if the local cytosol is highly viscoelastic, in principle, deformation of the object (induced by the motion of the cargo) might also oppose motion, so that the force applied by the trap would be only one component of the force opposing motion. Given the agreement between the in vitro single-molecule force and that measured here, it seems unlikely on average that viscoelastic opposition plays a large role in this system, but that obviously may not be true for all systems, or for each cargo, and it will be interesting to compare the in vivo stall forces from this method and the viscoelastic method in a variety of systems to understand when such opposition becomes a significant contributor to the overall properties of the systems.

SUPPORTING MATERIAL

REFERENCES

1. Ashkin, A. 1970. Acceleration and trapping of particles by radiation pressure. *Phys. Rev. Lett.* 24:156–159.

2. Block, S. M., L. S. Goldstein, and B. J. Schnapp. 1990. Bead movement by single kinesin molecules studied with optical tweezers. *Nature.* 348:348–352.

3. Mallik, R., B. C. Carter, …, S. P. Gross. 2004. Cytoplasmic dynein functions as a gear in response to load. *Nature.* 427:649–652.

4. Molloy, J. E., J. E. Burns, …, D. C. White. 1995. Movement and force produced by a single myosin head. *Nature.* 378:209–212.

5. Collin, D., F. Ritort, …, C. Bustamante. 2005. Verification of the Crooks fluctuation theorem and recovery of RNA folding free energies. *Nature.* 437:231–234.

6. Bérut, A., A. Arakelyan, …, E. Lutz. 2012. Experimental verification of Landauer's principle linking information and thermodynamics. *Nature.* 483:187–189.

7. Ashkin, A., K. Schütze, …, M. Schliwa. 1990. Force generation of organelle transport measured in vivo by an infrared laser trap. *Nature.* 348:346–348.

8. Wirtz, D. 2009. Particle-tracking microrheology of living cells: principles and applications. *Annu. Rev. Biophys.* 38:301–326.

9. Leidel, C., R. A. Longoria, …, G. T. Shubeita. 2012. Measuring molecular motor forces in vivo: implications for tug-of-war models of bidirectional transport. *Biophys. J.* 103:492–500.

10. Sims, P. A., and X. S. Xie. 2009. Probing dynein and kinesin stepping with mechanical manipulation in a living cell. *ChemPhysChem.* 10:1511–1516.

11. Hendricks, A. G., E. L. F. Holzbaur, and Y. E. Goldman. 2012. Force measurements on cargoes in living cells reveal collective dynamics of microtubule motors. *Proc. Natl. Acad. Sci. USA.* 109:18447–18452.

12. Mas, J., A. C. Richardson, …, K. Berg-Sørensen. 2013. Quantitative determination of optical trapping strength and viscoelastic moduli inside living cells. *Phys. Biol.* 10:046006.

13. Smith, S. B., Y. Cui, and C. Bustamante. 2003. Optical-trap force transducer that operates by direct measurement of light momentum. *Methods Enzymol.* 361:134–162.

14. Farré, A., and M. Montes-Usategui. 2010. A force detection technique for single-beam optical traps based on direct measurement of light momentum changes. *Opt. Express.* 18:11955–11968.

15. Farré, A., F. Marsà, and M. Montes-Usategui. 2012. Optimized back-focal-plane interferometry directly measures forces of optically trapped particles. *Opt. Express.* 20:12270–12291.

16. Mas, J., A. Farré, …, M. Montes-Usategui. 2011. Measuring stall forces in vivo with optical tweezers through light momentum changes. *Proc. SPIE.* 8097:809726.

17. Gross, S. P. 2003. Application of optical traps in vivo. *Methods Enzymol.* 361:162–174.

18. Gittes, F., and C. F. Schmidt. 1998. Interference model for back-focal-plane displacement detection in optical tweezers. *Opt. Lett.* 23:7–9.

19. Carter, B. C., G. T. Shubeita, and S. P. Gross. 2005. Tracking single particles: a user-friendly quantitative evaluation. *Phys. Biol.* 2:60–72.

20. Svoboda, K., and S. M. Block. 1994. Optical trapping of metallic Rayleigh particles. *Opt. Lett.* 19:930–932.

21. Berg-Sørensen, K., and H. Flyvbjerg. 2004. Power spectrum analysis for optical tweezers. *Rev. Sci. Instrum.* 75:594–612.

22. Tolić-Nørrelykke, S. F., E. Schäffer, …, H. Flyvbjerg. 2006. Calibration of optical tweezers with positional detection in the back focal plane. *Rev. Sci. Instrum.* 77:103101.

23. Svoboda, K., and S. M. Block. 1994. Biological applications of optical forces. *Annu. Rev. Biophys. Biomol. Struct.* 23:247–285.

24. Xu, J., B. J. N. Reddy, …, S. P. Gross. 2012. Casein kinase 2 reverses tail-independent inactivation of kinesin-1. *Nat. Commun.* 3:754.

25. Girifalco, L. A. 1955. Temperature dependence of viscosity and its relation to vapor pressure for associated liquids. *J. Chem. Phys.* 23:2446–2447.

26. Seol, Y., A. E. Carpenter, and T. T. Perkins. 2006. Gold nanoparticles: enhanced optical trapping and sensitivity coupled with significant heating. *Opt. Lett.* 31:2429–2431.

27. Mao, H., J. R. Arias-Gonzalez, …, C. Bustamante. 2005. Temperature control methods in a laser tweezers system. *Biophys. J.* 89:1308–1316.

28. Swindells, J. F., C. F. Snyder, …, P. E. Golden. 1958. Viscosities of Sucrose Solutions at Various Temperatures: Tables of Recalculated Values. U. S. Department of Commerce, National Bureau of Standards, Washington, D.C.

29. Xu, J., Z. Shu, …, S. P. Gross. 2012. Tuning multiple motor travel via single motor velocity. *Traffic.* 13:1198–1205.

30. Svoboda, K., and S. M. Block. 1994. Force and velocity measured for single kinesin molecules. *Cell.* 77:773–784.

31. Schnitzer, M. J., K. Visscher, and S. M. Block. 2000. Force production by single kinesin motors. *Nat. Cell Biol.* 2:718–723.

32. Rai, A. K., A. Rai, …, R. Mallik. 2013. Molecular adaptations allow dynein to generate large collective forces inside cells. *Cell.* 152:172–182.

33. Vershinin, M., B. C. Carter, …, S. P. Gross. 2007. Multiple-motor based transport and its regulation by Tau. *Proc. Natl. Acad. Sci. USA.* 104:87–92.

34. Nishiyama, M., H. Higuchi, and T. Yanagida. 2002. Chemomechanical coupling of the forward and backward steps of single kinesin molecules. *Nat. Cell Biol.* 4:790–797.

35. Shubeita, G. T., S. L. Tran, …, S. P. Gross. 2008. Consequences of motor copy number on the intracellular transport of kinesin-1-driven lipid droplets. *Cell.* 135:1098–1107.

36. Schroeder, 3rd, H. W., A. G. Hendricks, …, E. L. Holzbaur. 2012. Force-dependent detachment of kinesin-2 biases track switching at cytoskeletal filament intersections. *Biophys. J.* 103:48–58.

37. Tomishige, M., D. R. Klopfenstein, and R. D. Vale. 2002. Conversion of Unc104/KIF1A kinesin into a processive motor after dimerization. *Science.* 297:2263–2267.

38. Campàs, O., C. Leduc, …, J. Prost. 2008. Coordination of kinesin motors pulling on fluid membranes. *Biophys. J.* 94:5009–5017.

39. Snider, J., F. Lin, …, S. P. Gross. 2004. Intracellular actin-based transport: how far you go depends on how often you switch. *Proc. Natl. Acad. Sci. USA.* 101:13204–13209.